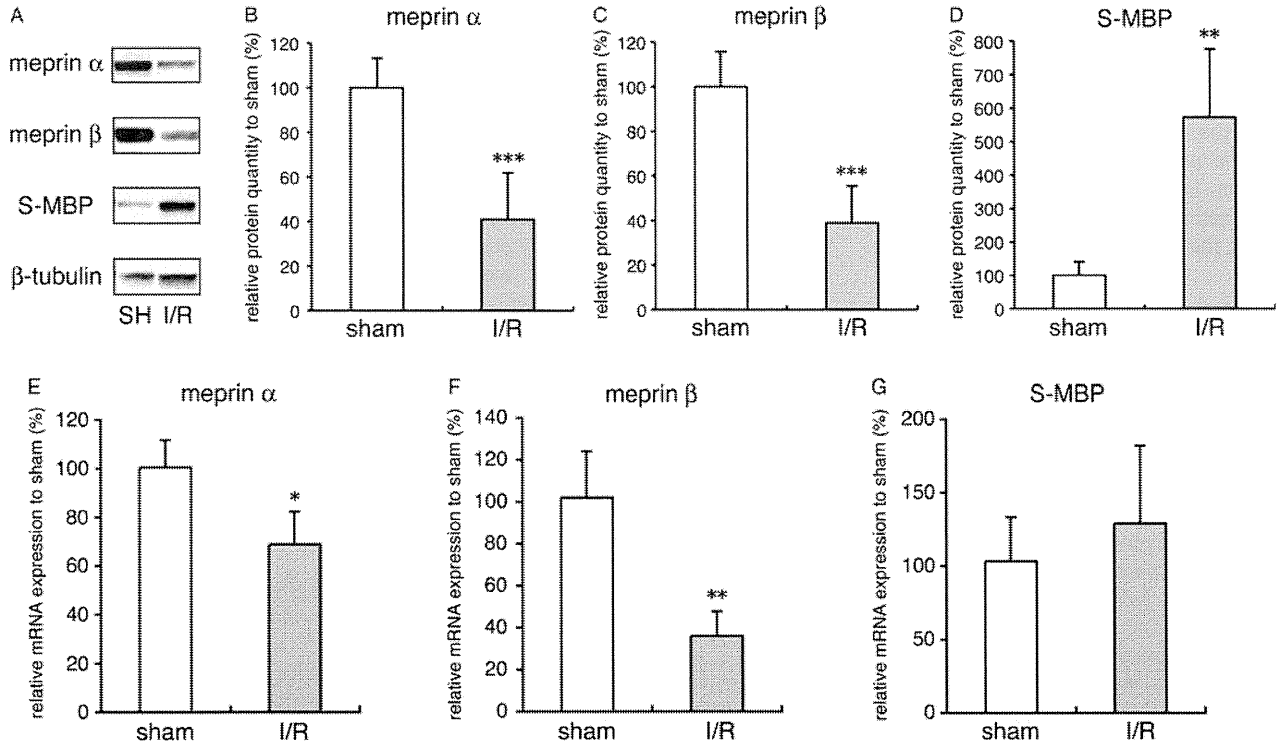

Fig. 5. Protein determination and mRNA levels of meprin α, meprin β and S-MBP in the I/R-operated mouse kidneys. (**A**) Western blotting analysis of meprins and S-MBP. SDS extracts of the renal cortex proteins of an I/R- and a sham (SH)-operated mouse were resolved on a 5–20% Tris–HCl gradient gel, and proteins, meprin α, meprin β, S-MBP and β-tubulin were detected by western blot analysis with their respective antibodies as described in *Materials and methods*. Relative protein levels of meprin α (**B**), meprin β (**C**) and S-MBP (**D**) were quantified as their band densities on western blotting analysis. Protein quantities were normalized as to the band density of β-tubulin. The data are expressed as means with SD ($n = 6$). (**E–G**) Total RNA was extracted from I/R- and sham-operated mouse kidney cortexes and subsequently reverse-transcribed with random hexamers. Real-time PCRs were performed with the resultant cDNA as a template, as described in *Materials and methods*. The mRNA expression of each was normalized as to the expression of GAPDH. The data are expressed as means with SD ($n = 6$). $^{*}P < 0.05$, $^{**}P < 0.005$ and $^{***}P < 0.001$.

proximal tubules and, therefore, it is reasonable to suppose that S-MBP can neither bind to the brush border membranes of the proximal tubules nor initiate complement activation.

Renal I/R operation significantly decreased the amounts of meprin proteins in the kidneys, whereas it increased the protein level of S-MBP, this being in complete agreement with the results of immunohistochemical analysis. Some years ago, we reported that S-MBP mRNA is expressed in the rat kidney (Morio et al. 1997). Then, we examined whether renal I/R increases the expression of S-MBP mRNA in the kidneys or not. The results of real-time PCR did not show significant changes of S-MBP mRNA expression in the I/R-operated mouse kidney. It was noted that the expression of S-MBP mRNA was slightly higher than that in the sham-operated kidney, suggesting the possibility that up-regulation of S-MBP mRNA expression may play some roles in this acute renal failure. This would be particularly so if the significantly down-regulated levels of meprins in the I/R-operated mouse kidney are taken into account. However, the markedly high level of S-MBP protein after the I/R operation may be explained most probably by the influx of S-MBP from the circulation. Although the glomerulus cannot filter out proteins that weigh >200 kDa (Tang et al. 2002) under the physiological condition, in the renal I/R-operated mouse kidney, this mechanism may not work properly.

Hemorrhagic shock or renal transplantation can lead to ischemic acute renal failure (Bonventre and Weinberg 2003). When the kidneys undergo ischemia, originally, the hypoxia damages the epithelial cells of the proximal tubules (Donohoe et al. 1978; Goligorsky et al. 1993). Additionally, the epithelial cells lose their polarity, and subsequently proteases that are normally localized on the apical surface of the epithelial cells are expressed on the basolateral membranes, where they degrade some extracellular matrix proteins (Kaushal et al. 1994; Fanning et al. 1999; Molitoris and Marrs 1999). This attenuates cell–cell or cell–matrix adhesion (Zuk et al. 1998). On the other hand, in the blood circulation of the kidney, some inflammatory mediators or cytokines, which are secreted by leukocytes activated by inflammation, facilitate vascular permeability (Bonventre and Zuk 2004). During this process, S-MBP can translocated to the proximal tubules from the blood circulation, interact with meprins on the brush border membranes of the proximal tubules, and then initiate the complement activation that results in necrosis of the tubular epithelial cells.

In conclusion, we demonstrate that S-MBP most probably derived from the blood circulation interacts with its endogenous ligands meprins in vivo in the I/R-operated mouse kidney and that the interaction initiates the complement activation through the MBP lectin pathway. These findings may contribute to the prevention of acute renal failure after renal transplantation, for example, by adding mannose as an inhibitor of the interaction of MBP with meprins to the preservation solution for the donor kidneys.

Materials and methods

Preparation of experimental renal I/R model mice

Six-week-old male BALB/c mice weighing 20–25 g were obtained from Japan SLC Inc. (Shizuoka, Japan) and were allowed free access to food and water during the experiments. The studies were carried out according to a protocol approved by the Institutional Animal Care Committee of Kyoto University. The experimental renal I/R model mice were prepared as described (Trachtman et al. 1995). In brief, mice were anesthetized with 45 mg/kg of sodium pentobarbital (Dainippon Sumitomo Pharma, Osaka, Japan). The body temperature was maintained at 37°C with a hot plate until the mice recovered from the anesthesia. An abdominal incision was made and ischemia was induced by bilateral renal artery clamping for 40 min. After removing the clamps, the wound was stitched up. The mice were sacrificed and their kidneys were removed for immunohistochemical analysis, protein quantification and real-time PCR at the indicated time points after ischemia. Sham-operated mice underwent the above-mentioned processes without renal artery clamping. During the operation, blood was sampled from the tail before ischemia, and 0, 1, 3, 6, 12 and 24 h after ischemia to quantitate BUN as an index of the severity of the acute renal failure using Urea N B (Wako, Osaka, Japan).

Immunohistochemical analysis

The I/R- and sham-operated kidneys were removed from mice that had been perfused with phosphate-buffered saline (PBS) and subsequently with PBS containing 4% (w/v) paraformaldehyde (PFA). The kidneys were fixed with 4% PFA/PBS overnight, dehydrated and then embedded in paraffin. Blocks were sectioned with a microtome (RM 2155; Leica, Wetzlar, Germany) at 10 μm and mounted on Matsunami adhesive silane-coated slides (Matsunami Glass Ind., Ltd., Osaka, Japan). Paraffin-embedded sections were deparaffinized with xylene and then hydrated with ethanol and PBS. Sections underwent microwave-stimulated antigen retrieval in 10 mM citrate buffer (pH 6.0) containing 1 mM ethylenediaminetetraacetic acid (EDTA) and then were rinsed with Tris-buffered saline (TBS) for 30 min. After blocking with horse serum (Vector Laboratories, Inc., Burlingame, CA), sections were incubated with 2.0 μg/mL goat anti-human meprin α or β polyclonal antibodies (R&D Systems, Minneapolis, MN) in TBS for 20 min at room temperature. Sections were washed in three changes of TBS containing 0.05% (v/v) Tween 20 (TBST) and then incubated with 1.0 μg/mL Alexa Fluor 546-labeled donkey anti-goat IgG (Invitrogen, Carlsbad, CA) in TBS for 30 min at room temperature. After washing in three changes of TBST, for double-immunofluorescence staining, sections were reacted with 10 μg/mL rat anti-mouse S-MBP mAb (8G6; Hycult Biotechnology, Uden, the Netherlands), 5 μg/mL rat anti-mouse L-MBP mAb (272801; R&D Systems) or 10 μg/mL rat anti-mouse C3b mAb (11H9; Abcam, Cambridge, MA) in TBS for 30 min at room temperature. Sections were washed in three changes of TBST and then incubated with 1.0 μg/mL Alexa Fluor 488-labeled rabbit anti-rat IgG (Invitrogen) in TBS for 30 min at room temperature. After washing in three changes of TBST again, sections were cover-slipped with Aqueous Mounting Medium PERMAFLUOR™ (Beckman Coulter, Marseille, France). Negative controls underwent staining with no primary antibodies. Fluorescent images were obtained under a confocal microscope, FluoView™ FV1000 (Olympus, Tokyo, Japan).

Chemical cross-linking, IP and immunoblotting

The I/R- and sham-operated kidneys were dissected from mice that had been perfused with PBS. Kidney cortexes were cut into small pieces. After washing three times with 0.1 M 2-[4-(2-hydroxyethyl)-1-piperazinyl]ethanesulfonic acid (HEPES, pH 7.4), pieces (40 mg) were subjected to cross-linking with 10 mM DSP (PIERCE, Rockford, IL) in 0.1 M HEPES (pH 7.4) for 30 min at room temperature, the reaction being stopped by adding 50 mM Tris–HCl (pH 7.5) to the reaction mixture followed by incubation for an additional 15 min at room temperature. Pieces were then washed three times with the homogenization buffer [150 mM NaCl, 20 mM Tris–HCl (pH 7.5), 1 mM EDTA and protease inhibitor cocktail (Nacalai Tesque, Kyoto, Japan)] and homogenized with a POLYTRON® (CH-6010; Kinematica, Luzernerstrasse, Switzerland) in 360 μL of the homogenization buffer. Homogenates were centrifuged (1000 × g, 10 min, 4°C) to remove cell debris and nuclei. Supernatants were solubilized with 1% (v/v) NP-40 and then centrifuged (105,000 × g, 1 h, 4°C). NP-40 lysates were incubated with 1 μg/mL goat anti-human meprin α (R&D Systems), 0.5 μg/mL goat anti-human meprin β polyclonal antibodies (R&D Systems) or 5 μg/mL anti-S-MBP mAb (8G6; Hycult Biotechnology), and complexes were precipitated with Protein G Sepharose 4B (GE Healthcare UK Ltd, Buckinghamshire, UK). Proteins bound to the beads were eluted with the SDS–PAGE sample buffer, resolved on a 5–20% Tris–HCl polyacrylamide gradient gel (ATTO, Tokyo, Japan) under non-reducing conditions and transferred to nitrocellulose membranes (Bio-Rad, Hercules, CA). Membranes were probed with anti-meprin α (R&D Systems), meprin β (R&D Systems) and anti-S-MBP antibody (8G6; Hycult Biotechnology), which recognizes only non-reduced forms of S-MBP, followed by HRP-conjugated respective secondary antibodies (Zymed, South San Francisco, CA) and developed by an enhanced chemiluminescence method (SuperSignal West Pico Chemiluminescent Substrate; PIERCE). Bands were visualized with a luminescent image analyzer, LAS-4000 mini (Fujifilm, Tokyo, Japan) and analyzed with standard image analysis software, MultiGauge ver. 3.0 (Fujifilm).

Detection of endogenous protein complexes in situ by proximity ligation

To investigate the in situ interaction between S-MBP and meprins, we performed the in situ PLA of paraffin sections of the I/R- and sham-operated mouse kidneys using Duolink™ in situ PLA (Olink Bioscience, Uppsala, Sweden) according to the manufacturer's instructions. In brief, sections, which had been deparaffinized, undergone microwave-stimulated antigen retrieval and blocked with horse serum (Vector Laboratories, Inc.), were incubated with 10 μg/mL rat anti-mouse S-MBP mAb (8G6; Hycult Biotechnology) and 2.0 μg/mL goat anti-human meprin α or β polyclonal antibodies (R&D Systems). After washing sections, they were reacted with the secondary antibodies conjugated with oligonucleotides (PLA probe MINUS for anti-S-MBP and PLA probe PLUS for anti-meprin α or β) for 2 h at 37°C. After washing sections with TBST, the two nucleotides were added to the hybridization buffer, followed by incubation for 15 min at 37°C to hybridize the two probes. Then the slides were washed with TBST and then reacted with ligase (1 U/section) for 15 min at 37°C to join the two hybridized oligonucleotides to close the circle when the PLA probes were in close proximity. A rolling-circle amplification (RCA) reaction that involves the formed circular oligonucleotide as a template was performed on sections for 90 min at 37°C by adding the nucleotides and polymerase (5 U/section) to generate a repeated sequence product extending from the oligonucleotide arm of the PLA probe. To detect the RCA product, Tex613 fluorophore-labeled oligonucleotide probes were hybridized to the RCA product for 60 min at 37°C. After washing with saline-sodium citrate buffer and 70% (v/v) ethanol, sections were cover-slipped with Aqueous Mounting Medium PERMAFLUOR™ (Beckman Coulter). Negative controls underwent staining with either anti-S-MBP or anti-meprin antibodies or with no primary antibodies. Fluorescent images were obtained under a confocal microscope, FluoView™ FV1000 (Olympus).

Purification of MBP from human serum, isolation of meprins from the mouse kidneys and preparation of biotin-labeled mouse meprins and human IgM Fc

Human MBP was purified from combined Cohn's fractions II and III, which had been prepared from healthy donors at Mitsubishi Pharma Co. (Osaka, Japan), by affinity chromatography on a mannan-agarose (Sigma-Aldrich, St Louis, MO) column, followed by a heparin-agarose (Tosoh, Tokyo, Japan) column as described previously (Nakamura et al. 2009). For the preparation of a Sepharose 4B-MBP column, human MBP was coupled to cyanogen bromide-activated Sepharose 4B (GE Healthcare UK Ltd), according to the manufacturer's instructions. Meprins were isolated from kidney membrane proteins with a Sepharose 4B-MBP column as described previously (Hirano et al. 2005). The isolated meprins and human IgM (Jackson ImmunoResearch Laboratories, Inc., West Grove, PA) were biotinylated with a FluoReporter Mini-Biotin-XX Protein Labeling Kit (Invitrogen) according to the manufacturer's instructions. The biotinylated proteins were used for the assay of the MBP lectin pathway.

Assay of complement activity through the MBP lectin pathway in vitro

The MBP lectin pathway was assayed essentially as described previously (Gadjeva et al. 2003). In brief, the microtiter wells of BD BioCoat™ Streptavidin Assay Plates (BD Biosciences, Bedford, MA) were coated with 1.0 μg aliquots of biotinylated meprins or IgM Fc in 100 μL of the coating buffer for 1 h at room temperature. Residual protein binding sites were blocked with 0.1% (w/v) human serum albumin in TBS for 1 h. After washing with TBST containing 10 mM $CaCl_2$ (TBST/Ca^{2+}), wells were filled with 100 μL of the MBP binding buffer with or without 1.5 μg of recombinant mouse S- or L-MBP (R&D Systems) at room temperature for 1.5 h. After washing with TBST/Ca^{2+} thoroughly, diluted MBP-deficient human serum was added to the wells to supply MASPs, followed by incubation overnight at 4°C. At the end of the incubation, 100 μL of 2 μg/mL human C4 (Sigma-Aldrich) diluted in C4 dilution buffer was added to each well, followed by incubation at 37°C for 1.5 h. Wells were washed with TBST/Ca^{2+}, and then the deposited C4b was detected by adding HRP-conjugated anti-human C4 mAb (Santa Cruz Biotechnology, Inc., Santa Cruz, CA) in TBST/Ca^{2+} at room temperature for 1 h. HRP activity was determined by adding 100 μL of the 3,3′,5,5′-tetramethylbenzidine liquid substrate system for ELISA (Sigma-Aldrich) to each well, and then plates were analyzed with a Multilabel Counter (PerkinElmer, Waltham, MA) at 450 nm. All experiments were performed in triplicate and were repeated three times.

Protein determination

The I/R- and sham-operated kidneys were dissected from mice that had been perfused with PBS. The kidney cortexes were cut into pieces weighing 50 mg and homogenized with POLYTRON® (CH-6010; Kinematica) in 450 μL of the homogenization buffer. Homogenates were centrifuged (1000 × *g*, 10 min, 4°C) to remove cell debris and nuclei. To each supernatant, one-fourth volume of 5× SDS–PAGE sample buffer [0.5 M Tris–HCl (pH6.8), 10% (w/v) SDS, 50% (v/v) glycerol and 0.005% (w/v) bromophenol blue with or without 25% (v/v) 2-mercaptethanol] was added and then the mixture was centrifuged (10,000 × *g*, 10 min, 4°C). Supernatants were resolved on a 5–20% Tris–HCl polyacrylamide gradient gel (ATTO), followed by transfer to nitrocellulose membranes (Bio-Rad). Membranes were incubated with 0.2 μg/mL goat anti-human meprin α polyclonal antibody (R&D Systems), 0.1 μg/mL goat anti-human meprin β polyclonal antibody (R&D Systems), 5 μg/mL rat anti-mouse S-MBP mAb (8G6; Hycult Biotechnology), 2 μg/mL anti-mouse L-MBP (272801; R&D Systems) or 0.1 μg/mL mouse anti-β-tubulin mAb (JDR.3B8; Sigma-Aldrich). For visualization, SuperSignal West Pico Chemiluminescence Kit (PIERCE) was used with HRP-conjugated secondary antibodies (Zymed). The luminescent bands were scanned with a luminescent image analyzer, LAS-4000 mini (Fujifilm) and analyzed with standard image analysis software, ImageJ ver. 1.44i.

Real-time PCR for measurement of mRNA expression

The I/R- and sham-operated kidneys were dissected from mice that had been perfused with diethyl

pyrocarbonate-treated PBS. Total RNA was extracted from the kidney cortexes with an RNeasy® Micro Kit (QIAGEN GmbH, Hilden, Germany), treated with an RNase-free DNase set (QIAGEN GmbH) and subsequently reverse-transcribed with a SuperScript® First-Strand Synthesis System for RT–PCR (Invitrogen) using random hexamers as primers according to the manufacturer's instructions. The resultant cDNA was used as the template for real-time PCR with gene-specific primers (Hokkaido System Science, Hokkaido, Japan). The sequences of the primers were as follows: meprin α, 5′-AGA GAC ATC CCA GCA GAC AGA AG-3′ (forward primer) and 5′-CCA TTC CCT TTA CGT TCA CAG A-3′ (reverse primer); meprin β, 5′-CGG CAT CAG CCT TGG TTT-3′ (forward primer) and 5′-TGT CTT GGT CAA TTC CTC CAT CT-3′ (reverse primer); S-MBP, 5′-GAA GGG AGA ACC AGG TCA AGG GC-3′ (forward primer) and 5′-CAT TGA GAA GGC ATG CAA CTT GTT-3′ (reverse primer); and GAPDH, 5′-GGA GAA ACC TGC CAA GTA TGA TG-3′ (forward primer) and 5′-TGG AAG AGT GGG AGT TGC TGT-3′ (reverse primer). Real-time PCRs were performed with ABI Prism® 7000 (Applied Biosystems, Lincoln Centre Drive Foster City, CA) in the presence of 30 μM each primer and 25 μL of FastStart Universal SYBR Green Master Mix (ROX) (Roche, Basel, Switzerland) in a total volume of 50 μL. The following PCR conditions were used for all samples: 95°C for 10 min, and then 37 cycles of 95°C for 15 s and 60° C for 30 s. The fluorescence intensity was monitored at the end of each amplification step. At the end of the reactions, the melting curves and quantities were analyzed with Sequence Detection System Software ver. 1.0 (Applied Biosystems).

Statistical analysis

Data are expressed as the means with SD and statistical analysis was performed with Microsoft® Excel 2004 for Mac® (Microsoft, Redmond, WA) by means of Student's *t*-test. $P < 0.05$ was taken to denote statistical significance.

Funding

This work was supported by Grant-in-Aid for Scientific Research on Priority Areas (14082203 to T.K.) from the Ministry of Education, Culture, Sports, Science and Technology of Japan; Grants-in-Aid for Scientific Research (C-20590074 to N.K. and B-18370057 to T.K.), Core-to-Core Program-Strategic Research Networks (17005), from the Japan Society for the Promotion of Sciences.

Acknowledgements

The authors thank Masaomi Nangaku, M.D., Ph.D. (Division of Nephrology and Endocrinology, University of Tokyo School of Medicine), for the helpful discussions and critical comments; Mr. Masahiro Hirata (Department of Diagnostic Pathology, Kyoto University Hospital) for the guidance in the preparation of paraffin sections; Mikio Nishizawa, M.D., Ph.D. (Department of Bioscience and Biotechnology, Ritsumeikan University), for the technical advice regarding real-time PCR; and Ms. Tomoko Tominaga for the secretarial assistance.

Conflict of interest

None declared.

Abbreviations

BUN, blood urea nitrogen; DSP, dithiobis(succinimidylpropionate); EDTA, ethylenediaminetetraacetic acid; ELISA, enzyme-linked immunosorbent assay; GAPDH, glyceraldehyde-3-phosphate dehydrogenase; HEPES, 2-[4-(2-hydroxyethyl)-1-piperazinyl]ethanesulfonic acid; HRP, horseradish peroxidase; Ig, immunoglobulin; IP, immunoprecipitation; I/R, ischemia/reperfusion; L-MBP, liver-type MBP; mAb, monoclonal antibody; MASP, MBP-associated serine protease; MBL, mannan-binding lectin; MBP, mannan-binding protein; mRNA, messenger RNA; NP-40, Nonidet P-40; PAGE, polyacrylamide gel electrophoresis; PBS, phosphate-buffered saline; PCR, polymerase chain reaction; PFA, paraformaldehyde; PLA, proximity ligation assay; RCA, rolling-circle amplification; SDS, sodium dodecyl sulfate; S-MBP, serum-type MBP; TBS, Tris-buffered saline; TBST, TBS with Tween 20.

References

Bond JS, Beynon RJ. 1986. Meprin: A membrane-bound metalloendopeptidase. *Curr Top Cell Regul.* 28:263–290.

Bonventre JV, Weinberg JM. 2003. Recent advances in the pathophysiology of ischemic acute renal failure. *J Am Soc Nephrol.* 14:2199–2210.

Bonventre JV, Zuk A. 2004. Ischemic acute renal failure: An inflammatory disease? *Kidney Int.* 66:480–485.

Bylander J, Li Q, Ramesh G, Zhang B, Reeves WB, Bond JS. 2008. Targeted disruption of the meprin metalloproteinase beta gene protects against renal ischemia-reperfusion injury in mice. *Am J Physiol Renal Physiol.* 294: F480–F490.

de Vries B, Walter SJ, Peutz-Kootstra CJ, Wolfs TG, van Heurn LW, Buurman WA. 2004. The mannose-binding lectin pathway is involved in complement activation in the course of renal ischemia-reperfusion injury. *Am J Pathol.* 165:1677–1688.

Donohoe JF, Venkatachalam MA, Bernard DB, Levinsky NG. 1978. Tubular leakage and obstruction after renal ischemia: Structural-functional correlations. *Kidney Int.* 13:208–222.

Fanning AS, Mitic LL, Anderson JM. 1999. Transmembrane proteins in the tight junction barrier. *J Am Soc Nephrol.* 10:1337–1345.

Gadjeva M, Thiel S, Jensenius JC. 2003. Assays for the mannan-binding lectin pathway. *Curr Prot Immunol.* 13.6:1–8.

Goligorsky MS, Lieberthal W, Racusen L, Simon EE. 1993. Integrin receptors in renal tubular epithelium: New insights into pathophysiology of acute renal failure [editorial]. *Am J Physiol.* 264:F1–F8.

Gorbea CM, Flannery AV, Bond JS. 1991. Homo- and heterotetrameric forms of the membrane-bound metalloendopeptidases meprin A and B. *Arch Biochem Biophys.* 290:549–553.

Gorbea CM, Marchand P, Jiang W, Copeland NG, Gilbert DJ, Jenkins NA, Bond JS. 1993. Cloning, expression, and chromosomal localization of the mouse meprin beta subunit. *J Biol Chem.* 268:21035–21043.

Hansen S, Thiel S, Willis A, Holmskov U, Jensenius JC. 2000. Purification and characterization of two mannan-binding lectins from mouse serum. *J Immunol.* 164:2610–2618.

Hirano M, Ma BY, Kawasaki N, Okimura K, Baba M, Nakagawa T, Miwa K, Kawasaki N, Oka S, Kawasaki T. 2005. Mannan-binding protein blocks the activation of metalloproteases meprin α and β. *J Immunol.* 175:3177–3185.

Ishmael FT, Noreum MT, Benkovic SJ, Bond JS. 2001. Multimeric structure of the secreted meprin A metalloproteinase and characterization of the functional protomer. *J Biol Chem.* 276:23207–23211.

Kaushal GP, Walker PD, Shah SV. 1994. An old enzyme with a new function: Purification and characterization of a distinct matrix-degrading metalloproteinase in rat kidney cortex and its identification as meprin. *J Cell Biol.* 126:1319–1327.

Liu H, Jensen L, Hansen S, Petersen SV, Takahashi K, Ezekowitz AB, Hansen FD, Jensenius JC, Theil S. 2001. Characterization and quantification of mouse mannan-binding lectins (MBL-A and MBL-C) and study of acute phase responses. *Scand J Immunol.* 53:489–497.

Marchand P, Tang J, Bond JS. 1994. Membrane association and oligomeric organization of the alpha and beta subunits of mouse meprin A. *J Biol Chem.* 269:15388–15393.

Molitoris BA, Marrs J. 1999. The role of cell adhesion molecules in ischemic acute renal failure. *Am J Med.* 106:583–592.

Møller-Kristensen M, Wang W, Ruseva M, Thiel S, Nielsen S, Takahashi K, Shi L, Ezekowitz A, Jensenius JC, Gadjeva M. 2005. Mannan-binding lectin recognizes structures on ischemic reperfused mouse kidneys and is implicated in tissue injury. *Scand J Immunol.* 61:426–434.

Morio H, Kurata H, Katsuyama R, Oka S, Kozutsumi Y, Kawasaki T. 1997. Renal expression of serum-type mannan-binding protein in rat. *Eur J Biochem.* 243:770–774.

Nakamura N, Nonaka M, Ma BY, Matsumoto S, Kawasaki N, Asano S, Kawasaki T. 2009. Characterization of the interaction between serum mannan-binding protein and nucleic acid ligands. *J Leukoc Biol.* 86:737–748.

Park P, Haas M, Cunningham PN, Bao L, Alexander JJ, Quigg RJ. 2002. Injury in renal ischemia-reperfusion is independent from immunoglobulins and T lymphocytes. *Am J Physiol.* 282:F352–F357.

Phaneuf LR, Lillie BN, Hayes MA, Turner PV. 2007. Binding of mouse mannan-binding lectins to different bacterial pathogens of mice. *Vet Immunol Immunopathol.* 118:129–133.

Söderberg O, Gullberg M, Jarvius M, Ridderstråle K, Leuchowius KJ, Jarvius J, Wester K, Hydbring P, Bahram F, Larsson LG, et al. 2006. Direct observation of individual endogenous protein complexes *in situ* by proximity ligation. *Nat Methods.* 3:995–1000.

Tang S, Lai KN, Sacks SH. 2002. Role of complement in tubulointerstitial injury from proteinuria. *Kidney Blood Press Res.* 25:120–126.

Thadhani R, Pascual M, Bonventre JV. 1996. Acute renal failure. *N Engl J Med.* 334:1448–1460.

Trachtman H, Valderrama E, Dietrich JM, Bond JS. 1995. The role of meprin A in the pathogenesis of acute renal failure. *Biochem Biophys Res Commun.* 208:498–505.

Wagner S, Lynch NJ, Walter W, Schwaeble WJ, Loos M. 2003. Differential expression of the murine mannose-binding lectins A and C in lymphoid and nonlymphoid organs and tissues. *J Immunol.* 170:1462–1465.

Zhang M, Takahashi K, Alicot EM, Vorup-Jensen T, Kessler B, Thiel S, Jensenius JC, Ezekowitz RA, Moore FD, Carroll MC. 2006. Activation of the lectin pathway by natural IgM in a model of ischemia/reperfusion injury. *J Immunol.* 177:4727–4734.

Zuk A, Bonventre JV, Brown D, Martin KS. 1998. Polality, integrin and extracellular matrix dynamics in the post-ischemic rat kidney. *Am J Physiol Cell Physiol.* 275:C711–C731.

Cell Medicine, Vol. 4, pp. 125–147, 2013
Printed in the USA.

2155-1790/13 $90.00 + .00
DOI: http://dx.doi.org/10.3727/215517912X658918
www.cognizantcommunication.com

Human Decidua-Derived Mesenchymal Cells Are a Promising Source for the Generation and Cell Banking of Human Induced Pluripotent Stem Cells

Tomoko Shofuda,* Daisuke Kanematsu,† Hayato Fukusumi,† Atsuyo Yamamoto,*
Yohei Bamba,‡ Sumiko Yoshitatsu,§ Hiroshi Suemizu,¶ Masato Nakamura,¶#
Yoshikazu Sugimoto,** Miho Kusuda Furue,†† Arihiro Kohara,‡‡ Wado Akamatsu,‡
Yohei Okada,‡§§ Hideyuki Okano,‡ Mami Yamasaki,¶¶##*** and Yonehiro Kanemura†##

*Division of Stem Cell Research, Institute for Clinical Research, Osaka National Hospital,
National Hospital Organization, Chuo-ku, Osaka, Japan
†Division of Regenerative Medicine, Institute for Clinical Research,
Osaka National Hospital, National Hospital Organization, Osaka, Japan
‡Department of Physiology, Keio University School of Medicine, Shinjuku-ku, Tokyo, Japan
§Department of Plastic Surgery, Osaka National Hospital, National Hospital Organization, Osaka, Japan
¶Biomedical Research Department, Central Institute for Experimental Animals, Kawasaki-ku, Kawasaki, Japan
#Department of Pathology and Regenerative Medicine, Tokai University School of Medicine, Isehara, Kanagawa, Japan
**Division of Chemotherapy, Faculty of Pharmacy, Keio University, Minato-ku, Tokyo, Japan
††Laboratory of Stem Cell Cultures, Laboratory of Cell Cultures, Department of Disease Bioresources Research,
National Institute of Biomedical Innovation, Ibaraki, Osaka, Japan
‡‡JCRB Cell Bank, Laboratory of Cell Cultures, Research on Disease Bioresources,
National Institute of Biomedical Innovation, Osaka, Japan
§§Kanrinmaru-Project, School of Medicine, Keio University, Tokyo, Japan
¶¶Division of Molecular Medicine, Institute for Clinical Research,
Osaka National Hospital, National Hospital Organization, Osaka, Japan
##Department of Neurosurgery, Osaka National Hospital, National Hospital Organization, Osaka, Japan
***Department of Pediatric Neurosurgery, Takatsuki General Hospital, Takatsuki, Osaka, Japan

Placental tissue is a biomaterial with remarkable potential for use in regenerative medicine. It has a three-layer structure derived from the fetus (amnion and chorion) and the mother (decidua), and it contains huge numbers of cells. Moreover, placental tissue can be collected without any physical danger to the donor and can be matched with a variety of HLA types. The decidua-derived mesenchymal cells (DMCs) are highly proliferative fibroblast-like cells that express a similar pattern of CD antigens as bone marrow-derived mesenchymal cells (BM-MSCs). Here we demonstrated that induced pluripotent stem (iPS) cells could be efficiently generated from DMCs by retroviral transfer of reprogramming factor genes. DMC-hiPS cells showed equivalent characteristics to human embryonic stem cells (hESCs) in colony morphology, global gene expression profile (including human pluripotent stem cell markers), DNA methylation status of the OCT3/4 and NANOG promoters, and ability to differentiate into components of the three germ layers in vitro and in vivo. The RNA expression of XIST and the methylation status of its promoter region suggested that DMC-iPSCs, when maintained undifferentiated and pluripotent, had three distinct states: (1) complete X-chromosome reactivation, (2) one inactive X-chromosome, or (3) an epigenetic aberration. Because DMCs are derived from the maternal portion of the placenta, they can be collected with the full consent of the adult donor and have considerable ethical advantages for cell banking and the subsequent generation of human iPS cells for regenerative applications.

Key words: Induced pluripotent stem cells (iPSCs); Decidua; Mesenchymal cells; X-chromosome inactivation

INTRODUCTION

Great breakthroughs in cell reprogramming technology have led to the generation of induced pluripotent stem cells (iPSCs) and dramatic advances in stem cell research (43). To date, iPSCs have been generated efficiently from various accessible human tissues, including

Received May 31, 2012; final acceptance September 30, 2012. Online prepub date: November 1, 2012.
Address correspondence to Yonehiro Kanemura, M.D., Ph.D., Division of Regenerative Medicine, Institute for Clinical Research,
Osaka National Hospital, National Hospital Organization, 2-1-14 Hoenzaka, Chuo-ku, Osaka 540-0006, Japan.
Tel: +81-6-6942-1331; Fax: +81-6-6946-3530; E-mail: kanemura@onh.go.jp

dermal fibroblasts (22,27,37,42,47), blood cells (9,10,21), neural stem cells (6,19), mesenchymal stem cells (MSCs) (4,33,35), and keratinocytes (1). It is generally accepted that iPSCs are likely to contribute not only to the realization of regenerative medicine through the use of pluripotent stem cells but also to the elucidation of the molecular pathogenesis of many intractable diseases. The promise of therapies using human iPSCs (hiPSCs) has driven an intense search for good cell sources (34).

Human placenta is a fetal adnexal tissue that contains extraembryonic cells. It is composed of three layers: the amnion and the chorion, which are of fetal origin, and the decidua, which is of maternal origin. Fibroblast-like adherent cells isolated from various components of the fetal adnexa, including the placenta, show multipotency or pluripotency, suggesting that the fetal adnexa represents a new source of human stem cells (3,8,14,46). We recently isolated adherent cells from human term decidua vera, that is, decidua-derived mesenchymal cells (DMCs), and reported some of their properties (18). DMCs are highly proliferative fibroblast-like cells of purely maternal origin, and they express a similar pattern of cluster of differentiation (CD) antigens as bone marrow-derived mesenchymal cells (BM-MSCs). DMCs differentiate well into chondrocytes and moderately into adipocytes, but hardly at all into osteoblasts, in vitro (18). The high-proliferative ability of DMCs makes them relatively easy to prepare and maintain, and their derivation from the maternal portion of the human placenta, which is otherwise discarded, resolves many ethical concerns. These unique properties of DMCs give them several advantages for clinical use, and support their potential as an attractive alternative to allogeneic human stem cells for use in regenerative medicine (15,18).

In this study, we asked whether DMCs could be reprogrammed into hiPSCs and acquire pluripotency. The four reprogramming factors octamer-binding transcription factor 3/4 (OCT3/4), sex-determining region Y box 2 (SOX2), Krüppel-like factor 4 (KLF4), and myelocytomatosis viral oncogene homolog (MYC; OSKM), carried by retroviral vectors (42), were used to reprogram several lines of DMCs. The resulting hiPSCs closely resembled human embryonic stem cells (hESCs) in their morphology, and they expressed hESC markers, which are low or undetectable in native DMCs. These hiPSCs formed embryoid bodies in vitro and teratomas in vivo that contained components of all three germ layers. We think these unique properties of DMCs give them several advantages for clinical use and that the generation of hiPSCs from DMCs could lead to the establishment of hiPSC-banking systems. Such systems would increase the availability of allogeneic hiPSCs, because tissues expressing a wide array of human leukocyte antigen (HLA) variants could be banked for clinical applications.

MATERIALS AND METHODS

Human Tissues and Cells

This study was carried out in accordance with the principles of the Helsinki Declaration, and approvals to use human tissues were obtained from the ethical committee of Osaka National Hospital (No. 72, No. 109, and No. 110). The donor bloods were serologically tested for hepatitis B and C, human immunodeficiency virus (HBs, HCV, HIV), and syphilis. Full-term placental tissues, infant skin samples obtained during plastic surgery, and the results of donor blood tests were collected at the Osaka National Hospital with written informed consent.

Human ESCs (clone KhES1) were obtained from Kyoto University (Kyoto, Japan) (41) and propagated at Keio University in accordance with Japanese guidelines on the utilization of hESCs, under approval of the Ministry of Education, Culture, Sports, Science and Technology (MEXT) of Japan and the ethical committee of Keio University. Human iPSCs (clone 201B7) (42) were obtained from the RIKEN Cell Bank (Tsukuba, Japan).

Human Primary Cell Culture

Human DMCs were propagated from human term decidua vera, in Dulbecco's modified Eagle's medium (DMEM)/F-12 (1:1) supplemented with 10% fetal bovine serum (FBS), HEPES (15 mM), and antibiotic–antimycotic solution (Invitrogen, Carlsbad, CA, USA) at 37°C in 5% CO_2 as previously described (18,28). Human amnion-derived epithelial cells (AECs), human amnion-derived mesenchymal cells (AMCs), and human primary BM-MSCs were also propagated as previously described (18). Human primary dermal fibroblast cells (DFBs) were isolated from the toe skin tissue of infants with polydactyly and cultured in DMEM/F-12 (1:1) with 10% fetal bovine serum (FBS).

Generation and Culture of hiPSCs

Four pMX retroviral vectors encoding the reprogramming factors (OSKM) were obtained from Addgene, Inc. (Cambridge, MA, USA) (42). Amphotropic retroviruses were produced by the transfection of Platinum-A retroviral packaging cells (Cell Biolabs, Inc., San Diego, CA, USA) using FuGENE® 6 Transfection Reagent (Roche Diagnostics, Indianapolis, IN, USA). Host cells were infected with the retrovirus supernatants supplemented with polybrene (4 mg/ml, Nacalai Tesque, Kyoto, Japan). On day 5 postinfection, the cells were replated on mitomycin C-treated mouse embryonic fibroblast (MEF) feeder cells at a density of 2.5×10^4 cells/6-cm-diameter culture dish or 5×10^5 cells/10-cm culture dish. On the next day, the growth medium was replaced with hESC medium consisting of DMEM/F-12 (1:1) with 20% knockout serum replacement (KSR, Invitrogen)/2-mercaptoethanol (1 mM; Invitrogen)/basic fibroblast growth factor (bFGF; 5 ng/ml;

Wako Pure Chemical Industries, Ltd., Osaka Japan). The number of alkaline phosphatase (ALP)$^+$ colonies in a 6-cm culture dish was screened and estimated by staining with 1-Step™ NBT/BCIP reagent (Pierce Biotechnology, Rockford, IL, USA), according to the manufacturer's specifications at 28 days postinfection. Concurrently, human ESC-like colonies grown in the 10-cm culture dish were picked up around 30 days after gene induction. The colonies were clonally expanded for further analyses. Human ES cells (KhES1) and hiPSCs (201B7) were also propagated on feeder cells with hESC medium (41).

Quantitative Reverse Transcription-Polymerase Chain Reaction (qRT-PCR)

Total RNA was isolated using an RNeasy Mini kit (Qiagen, Valencia, CA, USA), and cDNAs were synthesized using a PrimeScript® First-Strand Synthesis Kit (Takara Bio, Inc., Shiga, Japan), according to the manufacturer's specifications. Quantitative PCR analysis was performed using gene-specific primers (Table 1) with Power SYBR® Green PCR Master Mix and the 7300 real-time PCR system (Applied Biosystems, Foster, CA, USA), and the comparative Ct or standard curve method

Table 1. Primers Used for RT-PCR and PCR

Description and Genes	Symbol	Gene ID		Primer Sequence (5′ to 3′)
Transgene detection				
POU class 5 homeobox 1	OCT3/4Tg	5460	S	CCCCAGGGCCCCATTTTGGTACC
			A	TTATCGTCGACCACTGTGCTGCTG
SRY (sex-determining region Y)-box 2	SOX2Tg	6657	S	GGCACCCCTGGCATGGCTCTTGGCTC
			A	TTATCGTCGACCACTGTGCTGCTG
v-Myc myelocytomatosis viral oncogene homolog	MYCTg	4609	S	CAACAACCGAAAATGCACCAGCCCCAG
			A	TTATCGTCGACCACTGTGCTGCTG
Krüppel-like factor 4	KLF4Tg	9314	S	ACGATCGTGGCCCCGGAAAAGGACC
			A	TTATCGTCGACCACTGTGCTGCTG
Expression of hES markers				
POU class 5 homeobox 1	OCT3/4	5460	S	GACAGGGGGAGGGGAGGAGCTAGG
			A	CTTCCCTCCAACCAGTTGCCCCAAAC
SRY (sex-determining region Y)-box 2	SOX2	6657	S	GGGAAATGGGAGGGGTGCAAAAGAGG
			A	TTGCGTGAGTGTGGATGGGATTGGTG
v-Myc myelocytomatosis viral oncogene homolog	MYC	4609	S	GCGTCCTGGGAAGGGAGATCCGGAGC
			A	TTGAGGGGCATCGTCGCGGGAGGCTG
Krüppel-like factor 4	KLF4	9314	S	ACGATCGTGGCCCCGGAAAAGGACC
			A	TGATTGTAGTGCTTTCTGGCTGGGCTCC
Nanog homeobox	NANOG	79923	S	GCAGAAGGCCTCAGCACCTA
			A	GGTTCCCAGTCGGGTTCAC
Telomerase reverse transcriptase	TERT	7015	S	CTCCATCCTGAAAGCCAAGAA
			A	CGAGTCAGCTTGAGCAGGAA
X (inactive)-specific transcript (nonprotein coding)	XIST	7503	S	TGGCAGGGAGTGCCAGCTCCA
			A	GACCAAGGTGCATGGCTGCGGT
Expression of endoderm markers				
Forkhead box A2	FOXA2	3170	S	TGCTGGTCGTTTGTTGTGG
			A	CATGTTGCTCACGGAGGAGTAG
GATA binding protein 4	GATA4	2626	S	CTCTTCAGGCAGTGAGAGCC
			A	GGTCCGTGCAGGAATTTGAGG
SRY (sex-determining region Y)-box 17	SOX17	64321	S	CCCATAGTTGGATTGTCAAAACC
			A	CACACCCAGGACAACATTTCTTT
α-Fetoprotein	AFP	174	S	TTGAGAAACCCACTGGAGATGA
			A	GTTATGTCTTCCCTCTTCACTTTGG
Albumin	ALB	213	S	GTTGCATGAGAAAACGCCAGTA
			A	AGCATGGTCGCCTGTTCAC
Expression of mesoderm markers				
T, brachyury homolog (mouse)	Brachyury	6862	S	TGGAATGCCTGCCCATC
			A	CCGTTGCTCACAGACCACA

(*continued*)

Table 1. Primers Used for RT-PCR and PCR (*Continued*)

Description and Genes	Symbol	Gene ID		Primer Sequence (5′ to 3′)
NK2 transcription factor related, locus 5	NKX2-5	1482	S	CCCCTGGATTTTGCATTCAC
			A	CGTGCGCAAGAACAAACG
Msh homeobox 1	MSX1	4487	S	CAGAAGATGCGCTCGTCAAA
			A	CGGCTTACGGTTCGTCTTG
Collagen, type II, α1	COL2A1	1280	S	GGAAGAGTGGAGACTACTGGATTGAC
			A	TCCATGTTGCAGAAAACCTTCA
Expression of neural markers				
Neurogenin 2	NEUROG2	63973	S	ATGCCTATTGTCCTGTCCTTCTCT
			A	TGACTTCTAACCTGCCCCTCTAAC
SRY (sex-determining region Y)-box 1	SOX1	6656	S	AGCAGTTGTTTCTGGAAGAGTCTGT
			A	AGGCCCTTATCCCGGACTAA
Paired box 6	PAX6	5080	S	ACCTGGCTAGCGAAAAGCAA
			A	CCCGTTCAACATCCTTAGTTTATCA
Expression of astrocyte marker				
Glial fibrillary acidic protein	GFAP	2670	S	ACATCGAGATCGCCACCTAC
			A	ACATCACATCCTTGTGCTCC
Expression of Epidermis marker				
Keratin 17	KRT17	3872	S	AGGAGATTGCCACCTACCG
			A	CTTGCCATCCTGGACCTCTT
Expression of other genes				
v-Myc myelocytomatosis viral oncogene homolog 1, lung carcinoma derived	MYCL1	4610	S	CGAGAGCCCAAGCGACTCGGAGAA
			A	CAGGGGGTCTGCTCGCACCG
GLIS family zinc finger 1	GLIS1	148979	S	TCTGCCCAGCCCACAAGGTTACCA
			A	GGCAGCGCTGTGGGGCATGA
GLIS family zinc finger 2	GLIS2	84662	S	CCGCTGTCCGACCTGCAGCA
			A	GGCTTCTCACCTGTGTGCGACCG
GLIS family zinc finger 3	GLIS3	169792	S	TGCTCACCAATGGGAAGCCGCG
			A	AGCCAAGAGCCCCTTTCCCAGGAT
Zinc finger and SCAN domain containing 4	ZSCAN4	201516	S	TCCACCTGCCTTAGTCCACGTCCA
			A	TGGGAGGGTGTCCCCATGTTTGCT
Internal control				
Glyceraldehyde-3-phosphate dehydrogenase	GAPDH	2597	S	CCACTTTGTCAAGCTCATTTCCT
			A	TCTCTTCCTCTTGTGCTCTTGCT
Bisulfite genomic sequencing PCR				
Nanog homeobox promoter	Bis-NANOG P	79923	S	GTTGGGTTTGTTTTTAGGTTTT
			A	CATAAAACAACCAACTCAATCC
POU class 5 homeobox 1 promoter	Bis-OCT3/4 P	5460	S	GTTAAGGTTAGTGGGTGGGATT
			A	AACATAAAAAAATCCCCCACA
Methylation-specific PCR				
Unmethylated-XIST promoter	Unmet-XIST P	7503	S	TTTTGTTGTAGTGTTTAAGTGGT
			A	AACCCACCATATTTTACACTACA
Methylated-XIST promoter	Met-XIST P	7503	S	TGTCGTAGTGTTTAAGTGGC
			A	CCGCCATATTTTACACTACG

S, sense primer; A, antisense primer.

(20). Total RNA isolated from various human tissues was used for controls (BD Biosciences, San Jose, CA, USA).

Microarray Analysis

The microarray study was carried out using the GeneChip array (Human Genome U133 Plus 2.0 gene expression array, Affymetrix, Inc., Santa Clara, CA, USA). One hundred nanograms of total RNA was used to synthesize amplified RNA (aRNA) using the 3′ IVT Express Kit, according to the manufacturer's instructions (Affymetrix). After aRNA purification, 15 μg of aRNA was fragmented and hybridized with a preequilibrated GeneChip array at 45°C for 16 h. The GeneChip array was then washed, stained, and scanned according to the manufacturer's instructions. The gene expression data were extracted using Affymetrix Expression Console software, and the

data sets were analyzed using GeneSpring GX software (Agilent Technologies, Inc., Santa Clara, CA, USA).

Flow cytometry (FCM) Analysis

Cells were preincubated with Y-27632 (Wako Pure Chemical Industries, Ltd.) for 30 min and then dissociated by trypsin/EDTA (Invitrogen). The dissociated cells were fixed with 4% paraformaldehyde (PFA) for 20 min on ice, washed with PBS, and then reacted with the following primary antibodies (Abs) for 30 min at 4°C: anti-stage-specific embryonic antigen 4 (SSEA-4) Ab (MC-813-70, Chemicon International, Inc., Temecula, CA, USA), anti-SSEA-3 Ab (MC-631, Chemicon), anti-TRA-1-60 Ab (TRA-1-60, Chemicon), or anti-TRA-1-81 Ab (TRA-1-81, Chemicon). After being washed, the cells were incubated with the appropriate secondary Abs (Alexa 488-conjugated anti-mouse IgG, anti-mouse IgM, or anti-rat IgM, Molecular Probes, Invitrogen) for 30 min at 4°C. The stained samples were analyzed by a FACSCalibur™ flow cytometer (BD Biosciences). All stainings were performed with matched-isotype controls.

Karyotype Analysis

Cells were cultured with colcemid (0.06 μg/ml; Invitrogen) at 37°C for 4 h, treated with Y-27632 to prevent apoptosis, and then dissociated with 0.05% trypsin/EDTA. The cells were incubated in KCl solution (75 mM) for 20 min and then fixed in Carnoy fluid. The fixed samples were heat-denatured at 95°C for 2 h, incubated in 0.025% trypsin for 10 s, and then stained with Giemsa (Merck, Darmstadt, Germany) for 7 min. The samples were observed with a microscope (Carl Zeiss, Hallbergmoos, Germany), and metaphase samples were analyzed using Ikaros (MetaSystems, Altlussheim, Germany).

Genotyping of Short-Tandem Repeat (STR) Polymorphisms

Genomic DNA (gDNA) was extracted by DNAzol Reagent (Invitrogen). STR loci were analyzed with the Powerplex 16 system (Promega, Madison, WI, USA) using an ABI PRISM3100 Genetic Analyzer (Applied Biosystems) and analyzed by GeneMapper software (Applied Biosystems) following the manufacturer's instructions (18).

Bisulfite Modification, DNA Sequencing, and Methylation-Specific PCR (MSP)

Genomic DNA was bisulfite-treated with an EZ DNA methylation-Gold Kit (Zymo Research, Irvine, CA, USA) according to the manufacturer's instructions. The promoter regions of human OCT3/4 and NANOG were amplified with specific primer sets (Table 1) by TaKaRa Taq™ Hot Start Version (Takara Bio, Inc.). The PCR products were subcloned into the pCR®2.1 vector (Invitrogen). Ten clones were sequenced with a universal primer using an ABI PRISM 3100 Genetic Analyzer (Applied Biosystems) and analyzed with Sequence analysis software (Applied Biosystems), following the manufacturer's instructions. Episcope® Methylated and Unmethylated HCT116 gDNA (Takara Bio, Inc.) were used as the control human genomic DNAs for the methylation analysis.

In Vitro Differentiation

Cells were incubated with 1 mg/ml collagenase type IV (Invitrogen) for 5 min at 37°C and harvested by scraper. The harvested colonies were broken into properly sized clumps by pipetting and then incubated on noncoated plates in human ES cell medium without bFGF to form embryoid bodies (EBs). After 10 days in floating culture, the EBs that formed were harvested for transcript analysis. Some of the EBs were transferred to gelatin-coated chamber slides (Nalge Nunc International, Rochester, NY, USA) and cultured for another 2 weeks (total 24 days) in DMEM supplemented with 10% FBS at 37°C in 5% CO_2.

Teratoma Formation Assay

NOG (non-obese diabetic/Shi-severe combined immunodeficient interleukin 2 receptor γ chain null; NOD/Shi-scid IL2Rγ null) mice (16) aged 6–8 weeks were maintained under specific pathogen-free conditions in the Animal Facility of the Central Institute for Experimental Animals (CIEA) in accordance with the guidelines of the Animal Care Committee at CIEA. All mouse studies were approved by the Animal Care Committee at CIEA. The recipient mice were anesthetized by isoflurane inhalation (Dainippon Pharmaceutical Co., Ltd., Osaka, Japan). Human iPSCs were transplanted into both subcutaneous tissue and kidney capsules. For the subcutaneous transplantation, hiPSCs (1×10^6 cells/0.1 ml of serum-free medium) were injected subcutaneously into the flank. For transplantation into the kidney capsule, the kidney was exteriorized through a dorsal–horizontal incision. A syringe fitted with a 29-G needle with a flattened tip was used. The needle was introduced into the kidney at a site apart from the transplanted region. The kidney was penetrated, and the tip of the needle was held just beneath the renal capsule. The suspension of hiPSCs (1×10^5 cells/10 μl of serum-free medium) was then injected underneath the kidney capsule. The mice were examined daily, and tumors were measured with calipers.

Teratoma samples were dissected and fixed with 4% (v/v) phosphate-buffered formalin, and paraffin-embedded sections were stained with hematoxylin and eosin using routine procedures (H&E staining).

Immunocytochemical and Immunohistochemical Staining

Cultured cells were fixed in 4% PFA, and tissue specimens were permeabilized with 0.1% Triton X-100. Nonspecific reactions were blocked with 10% normal goat serum. The samples were reacted with the following Abs overnight at 4°C: anti-α-fetoprotein (AFP) Ab (SantaCruz, Santa Cruz, CA, USA), anti-cytokeratin19 Ab (clone A53-B/A2, Santa Cruz), anti-desmin Ab (Thermo, Waltham, MA, USA), anti-α-smooth muscle actin (SMA) Ab (clone 1A4, Dako, Glostrup, Denmark), anti-glial fibrillary acidic protein (GFAP) Ab (Sigma, St. Louis, MO, USA), anti-βIII-tubulin Ab (clone TuJ1, Babco, Richmond, CA, USA), anti-vimentin Ab (Chemicon), anti-OCT3/4 Ab (Chemicon), and anti-NANOG Ab (Reprocell, Tokyo, Japan). The samples were then reacted with the appropriate secondary Abs (AlexaFluor®-488-conjugated goat anti-mouse IgG Ab, AlexaFluor®-568-conjugated goat anti-rabbit IgG Ab, Molecular Probes, Invitrogen), and TO-PRO-3® iodide (1 mM, Molecular Probes, Invitrogen) for 1 h at room temperature (RT).

The immunohistochemical staining of teratoma samples was carried out using an automated staining device with the Bond™ Polymer Refine Detection system (Leica Microsystems K.K., Tokyo, Japan) according to the manufacturer's instructions with minor modifications. In brief, 4-μm sections of formalin-fixed, paraffin-embedded tissues were deparaffinized with Bond™ Dewax Solution (Leica Microsystems), and antigen retrieval was performed using Bond™ ER Solution (Leica Microsystems) for 30 min at 100°C. Nonspecific peroxidase activity was quenched by incubating with 0.3% hydrogen peroxide for 5 min. The sections were incubated for 15 min at ambient temperature with the following Abs: anti-cytokeratin Ab (AE1/AE3, Leica Microsystems), anti-neural cell adhesion molecule (NCAM; CD56) Ab (1B6, Nichirei Bioscience, Tokyo, Japan), anti-desmin Ab (D33, Nichirei Bioscience), for 1 h at room temperature. The signals were detected by Bond™ Polymer Refine Detection (Leica Microsystems) with 3,3′-diaminobenzidine tetrahydrochloride (DAB; Dojindo Laboratories, Kumamoto, Japan) substrate as the chromogen. The sections were counterstained with hematoxylin.

The immune-stained preparations were examined using a confocal laser scanning microscope (LSM510, Carl Zeiss) or a light microscope (IX70, Olympus, Tokyo, Japan). All stainings were performed with matched isotype controls.

Statistical Analysis

Significant differences in the gene expression levels obtained by qRT-PCR were determined by analysis of variance (ANOVA) with post hoc comparisons. Details are provided in the figure legends.

RESULTS

Phenotype Analysis of Human Placenta-Derived Cells

To learn whether hiPSCs could be generated from placenta-derived cells by introducing retroviruses expressing the four reprogramming factors (OSKM), we first propagated three different kinds of somatic cells, DMCs, AECs, and AMCs, from human full-term placenta tissue (Fig. 1A) (18) and analyzed their endogenous expression of six pluripotent cell-specific marker genes in comparison with hESCs (KhES1), human primary DFBs, and human primary BM-MSCs (Fig. 1B). Quantitative RT-PCR analysis showed that c-MYC was expressed endogenously in all six cell types at the same level or higher than in hESCs and that the KLF4 levels were about the same in every cell type except DMCs (Fig. 1B). In contrast, the expression levels of the other four genes in five cell types (DFBs, AECs, AMCs, DMCs, and BM-MSCs) were significantly lower than in KhES1, to differing degrees (Fig. 1B).

Although AECs expressed higher levels of OCT3/4, NANOG, and SOX2 than the other four cell types (Fig. 1B) and thus seemed likely to be good candidate cells for generating hiPSCs (17), their growth was too slow (18) for them to be efficiently infected by retroviral vectors, and they were therefore excluded from further examination in this study.

Generation of iPSCs From Human DMCs

We next examined the gene transduction efficiency by amphotropic retrovirus infection. Three human primary cell types (DFBs, AMCs, and DMCs) were transduced with amphotropic retroviruses encoding the four reprogramming factors (OSKM), and OSKM transgene expression on day 3 postinfection was quantified by qRT-PCR (Fig. 2A). The expression of the exogenous reprogramming factors was two to three times higher in DMCs than DFBs ($p<0.01$) (Fig. 2A), and AMCs showed a comparable or lower expression than DFBs ($p<0.05$). On day 5 postinfection, the cells were split and replated on feeder cultures, and on day 28 postinfection, the reprogramming efficiency of each cell type was estimated by the number of ALP^+ (primary) colonies on 6-cm culture dishes. Approximately three times more primary colonies were generated from DMCs than AMCs, although the number was still half that generated from DFBs (Fig. 2B, top).

iPSCs of each cell type were generated from two 10-cm dishes containing 1×10^5 cells, infected as described above. The efficiency of hESC-like colony formation was determined by dividing the number of colonies with ESC-like morphology that emerged on the dishes by the number of seeded cells. The efficiency was

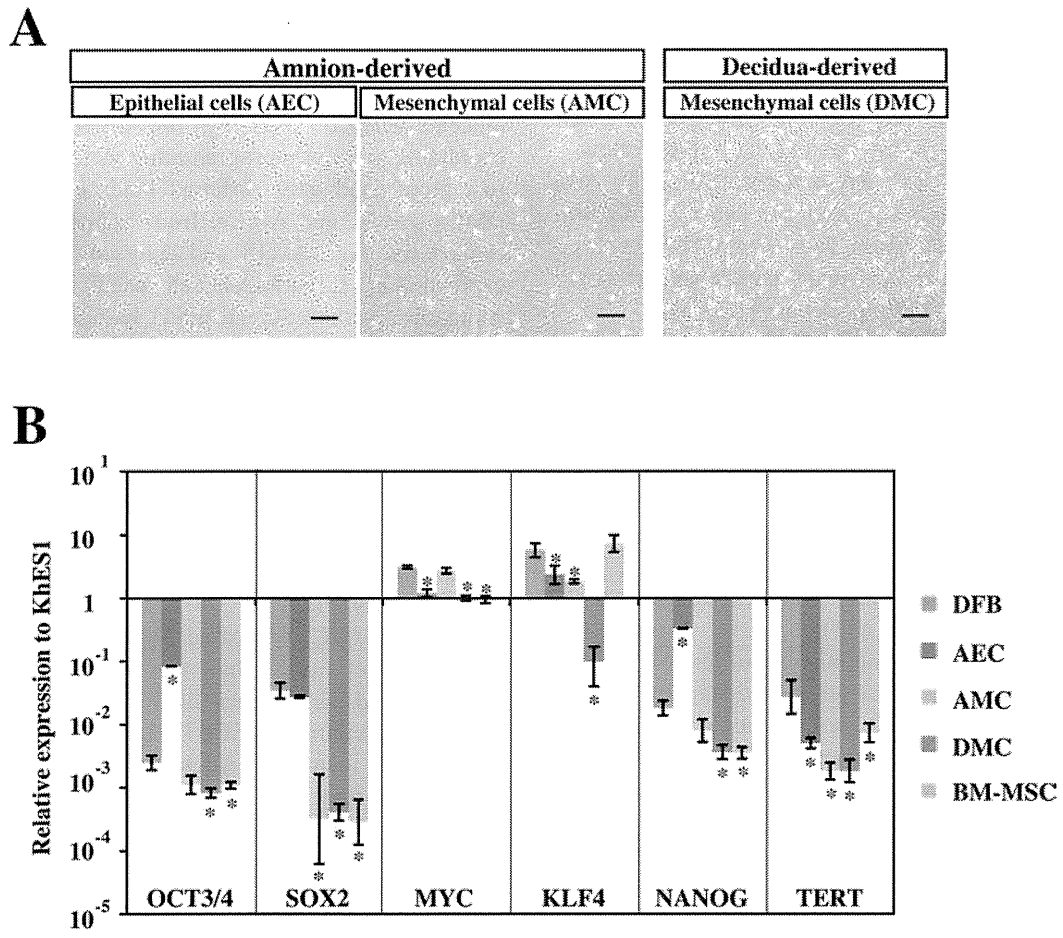

Figure 1. Phenotype analysis of human placenta-derived cells. (A) Phase contrast images of amnion-derived epithelial cells (AECs), amnion-derived mesenchymal cells (AMCs), and decidua-derived mesenchymal cells (DMCs). Scale bars: 200 μm. (B) Endogenous transcriptional expression of four reprogramming factors (OCT3/4, SOX2, KLF4, c-MYC) and pluripotent stem cell marker genes (NANOG and TERT). GAPDH was used as the internal control gene, and data are presented as the mean ± SD ($n=3$). Statistical significance was determined by Scheffe's test after ANOVA, and the p values between dermal fibroblast cells (DFBs) and other cells are shown (*$p<0.01$). See Table 1 for gene definitions. BM-MSCs, bone marrow-derived mesenchymal cells.

0.009 ± 0.002% for DFBs (mean ± SE, five independent experiments with five DFB lines), 0.020 ± 0.008% for AMCs (three independent experiments with two AMC lines), and 0.005 ± 0.001% for DMCs (12 experiments with eleven DMC lines), respectively.

We also examined the cellular properties of the morphologically hESC-like colonies generated on 10-cm culture dishes, as candidates for further analysis. After they were subcultured, approximately 90% of the colonies derived from primary colonies of DMCs retained both their hESC-like morphology and positive ALP activity after the second passage, whereas only 40% of the colonies from AMCs and DFBs met both conditions (Fig. 2B, bottom). Based on these findings, we selected DMCs as the first cells to use for iPSC generation.

Cellular Properties of DMC-hiPSCs

The DMC-hiPSC clones that retained their hESC-like morphology and positive ALP activity after several passages were also confirmed to express NANOG protein by immunocytochemistry (Fig. 3A). Expression analysis of the four transgenes by qRT-PCR analysis showed that each transgene was almost completely suppressed in two representative DMC-hiPSC clones (DMC5403 and DMC5413) compared with those on day 3 postinfection (Fig. 3B). To evaluate the protein levels of hESC markers, we analyzed two established clones and their parental DMCs (DMC54) by FCM. This analysis revealed that the two established clones highly expressed hESC-specific surface antigens (SSEA-3, SSEA-4, TRA-1-60, and TRA-1-81), whereas the parental DMCs showed little or

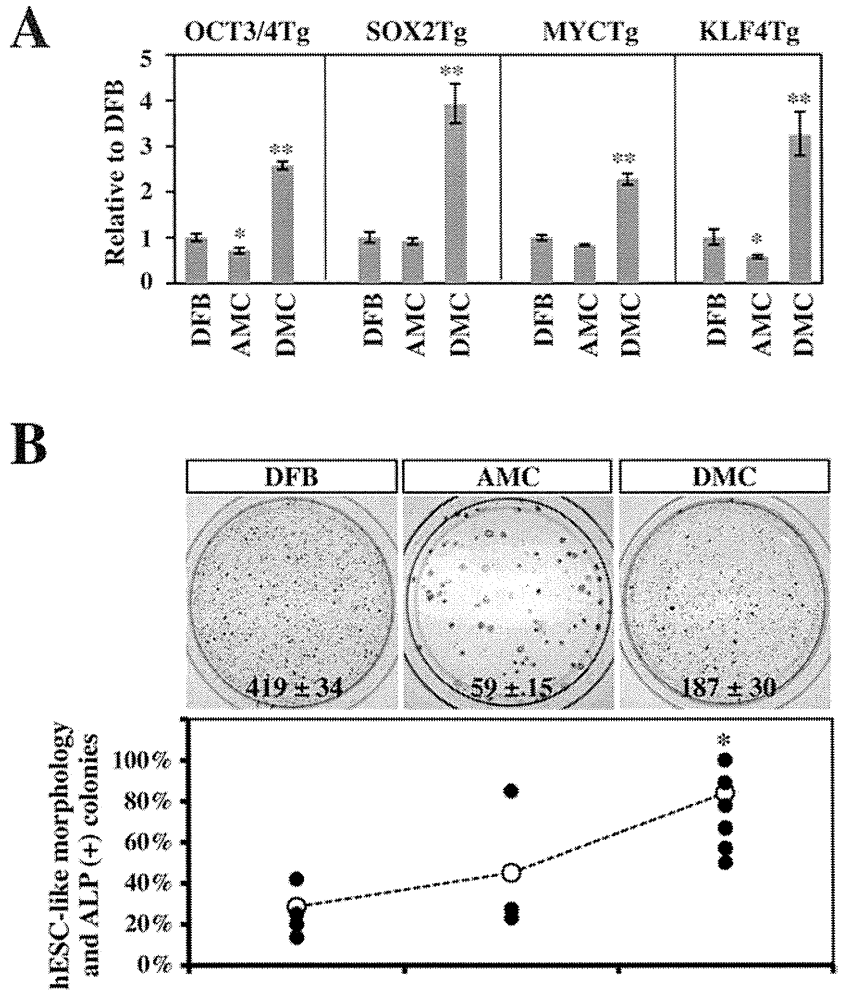

Figure 2. Efficiencies of gene transduction and generation of alkaline phosphatase (ALP)$^+$ colonies. (A) Gene transduction efficiencies of amphotropic retrovirus infection. Efficiencies were estimated on day 3 postinfection by qRT-PCR and are shown in comparison with those in DFBs (mean ± SD, 3 independent experiments). Statistical significance was determined by Scheffe's test after ANOVA (*$p<0.05$, **$p<0.01$). (B) Generation efficiency of ALP$^+$ colonies. (Top) Representative result of ALP$^+$ primary colonies (blue) emerging from 2.5×10^4 infected cells on a 6-cm culture dish (mean ± SD, 3 independent experiments). (Bottom) Efficiencies of retention of both the human embryonic stem cell (hESC)-like morphology and ALP activity in secondary colonies. Efficiency was determined by dividing the number of secondary colonies by the number of primary hESC-like colonies emerged on two 10-cm dishes. ●Independent results from 5 DFB experiments (DFB01, DFB18, DFB22, DFB37, and DFB44), 3 AMC experiments (AMC41 and a duplicate of AMC49), and 12 DMC experiments (DMC41 and duplicates of DMC54, DMC70, DMC71, DMC72, DMC73, DMC75, DMC76, DMC77, DMC83, and DMC92). ○Mean value. Statistical significance was determined by Scheffe's test after ANOVA (*$p<0.01$). See Table 1 for gene definitions.

no expression of these antigens, in comparison with the isotypic control antibody samples (Fig. 3C).

Karyotyping, Genotyping, and Promoter Methylation Analysis

Karyotyping by G band staining showed that both DMC-hiPSC clones had a normal female karyotype (46, XX) (Fig. 4A). Analysis of the methylation state of the OCT3/4 and NANOG promoters revealed that most of the CpG sites in the DMC-hiPSC clones were unmethylated, while those of the parental DMCs were highly methylated (Fig. 4B). Genotyping by STR-PCR showed a complete match of STRs between the parental DMCs and the two established clones (Table 2). These findings confirmed that the two DMC-hiPSC clones were derived from the parental DMCs and that their epigenetic status had been reprogrammed efficiently.

In Vitro Differentiation of DMC-hiPSCs

To confirm that the DMC-hiPSCs were pluripotent in vitro, we performed EB formation assays. The DMC-hiPSCs formed EBs in a 10-day suspension culture

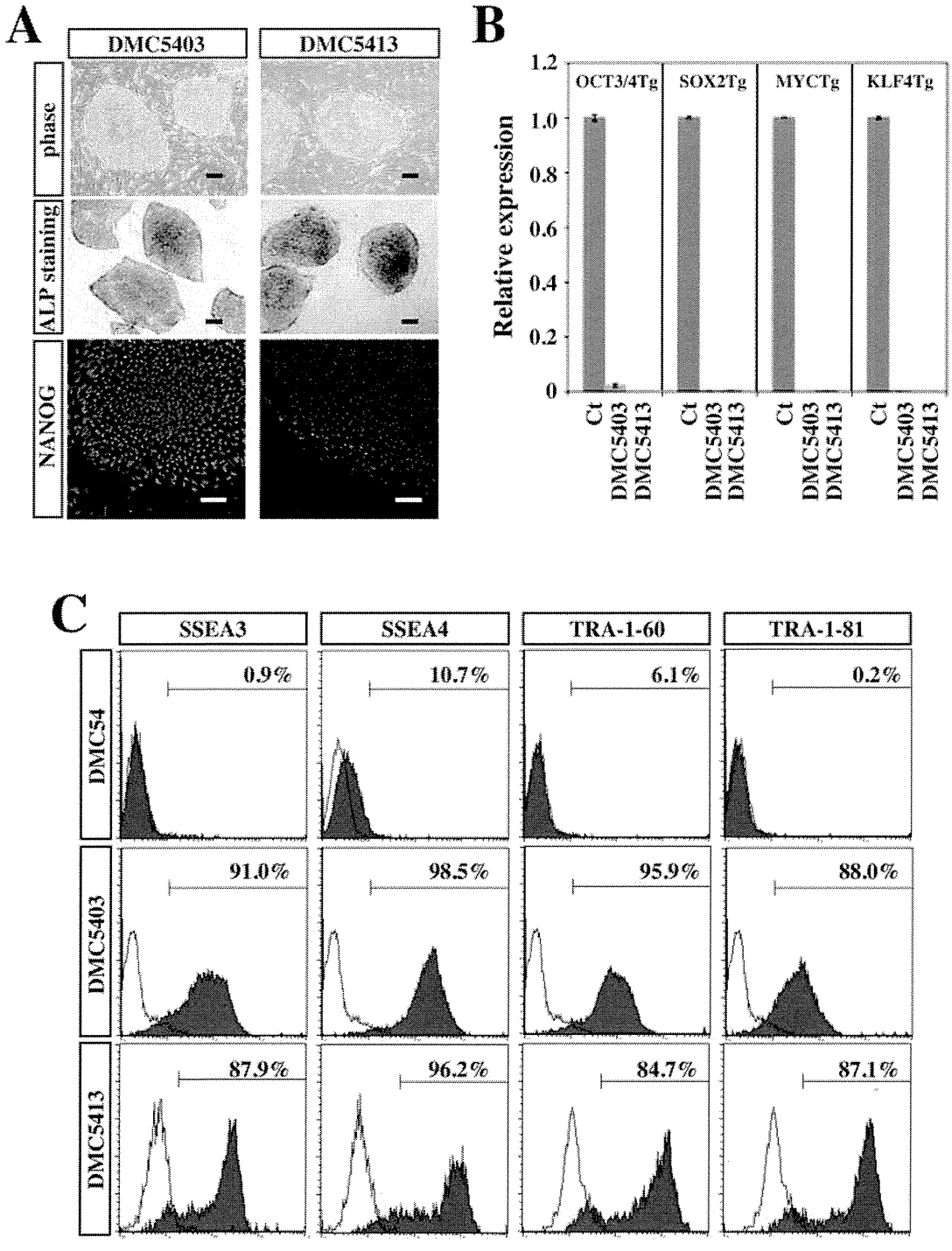

Figure 3. Characterization of decidua-derived mesenchymal cell-derived human induced pluripotent stem cells (DMC-hiPSCs). (A) Representative results of morphology and cytochemical analyses. Morphology (top), ALP staining (middle), and Nanog protein staining (bottom) of DMC-hiPSCs. Scale bar: 200 μm (morphology and ALP staining) and 50 μm (Nanog staining). (B) Expression of the four exogenous transgenes (OSKM) in DMC-hiPSC clones (DMC5403 and DMC5413) relative to infected cells extracted on day 3 postinfection (mean ± SD, 3 independent experiments). (C) Flow cytometry analysis of hESC-specific cell surface markers [stage-specific embryonic antigen 3 (SSEA3), SSEA4, TRA-1-60, and TRA-1-81]. The shaded histograms represent the distribution of cells stained by the respective antibodies, and the open histograms show the isotype control staining.

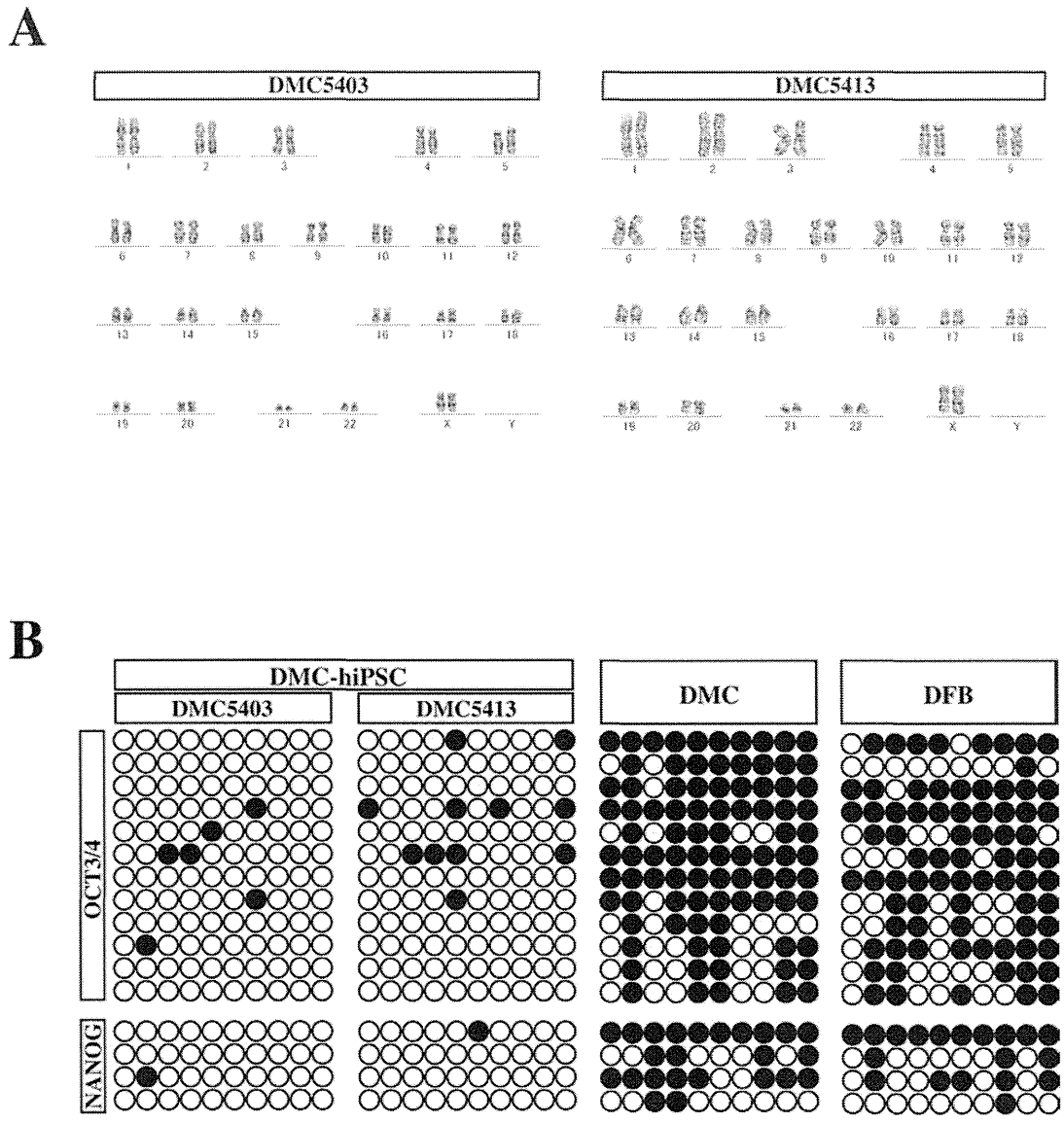

Figure 4. Genomic DNA analysis of DMC-hiPSCs. (A) Representative G-banding karyotype analysis of DMC-hiPSCs (DMC5403 and DMC5413). The DMC-hiPSC clones showed a normal karyotype at passage 30 and 38, respectively. (B) DNA methylation profile of the OCT3/4 and NANOG promoters in the DMC-hiPSCs, parental DMCs, and DFBs. ○Unmethylated CpGs; ●methylated CpGs.

(Fig. 5A), and qRT-PCR analysis showed the down-regulated expression of pluripotent stem cell marker genes [hESCs: OCT3/4, NANOG, and telomerase reverse transcriptase (TERT)] (Fig. 5B). The expression of differentiation-specific marker genes of the three germ layers [endoderm: forkhead box A2 (FOXA2), SOX17, AFP, and albumin (ALB); mesoderm: GATA binding protein 4 (GATA4), Brachyury, Mut S homolog (msh) homeobox 1 (MSX1), and NK2 transcription factor related, locus 5 (NKX2-5); ectoderm: neurogenin 2 (NEUROG2), SOX1, and paired box 6 (PAX6); epidermis: keratin 17 (KRT17)] was observed in these EBs (Fig. 5B). The expression levels of the differentiation-specific marker genes were equal to or surpassed those in EBs formed from 201B7 hiPSCs (Fig. 5B).

To confirm the progression of differentiation, we replated the 10-day-cultured EBs on gelatin-coated chamber slides, cultured them in 10% FBS-containing medium for an additional 2 weeks, and then examined the cells by immunocytochemistry on day 24 of total in vitro differentiation. On day 24, the cells in EBs had differentiated into various adherent cells, most of

Table 2. Short-Tandem Repeat (STR) Genotyping

Locus/Clone	DMC54	DMC5403	DMC5413	UCB54
Penta_E	18, 21	18, 21	18, 21	14, 18
D18S51	14, 16	14, 16	14, 16	14, 15
D21S11	31.2, 33.2	31.2, 33.2	31.2, 33.2	31.2, 33.2
TH01	9, 9	9, 9	9, 9	7, 9
D3S1358	15, 16	15, 16	15, 16	14, 15
FGA	19, 22	19, 22	19, 22	19, 23
TPOX	8, 9	8, 9	8, 9	8, 11
D8S1179	16, 16	16, 16	16, 16	10, 16
vWA	14, 16	14, 16	14, 16	16, 16
Amelogenin	X, X	X, X	X, X	X, Y
Penta_D	11, 15	11, 15	11, 15	11, 12
CSF1PO	11, 12	11, 12	11, 12	11, 11
D16S539	9, 12	9, 12	9, 12	9, 9
D7S820	8, 11	8, 11	8, 11	11, 12
D13S317	8, 8	8, 8	8, 8	8, 11
D5S818	11, 13	11, 13	11, 13	8, 11

Fifteen polymorphic STR DNA loci plus Amelogenin (AMEL) for sex chromosomes were analyzed.

which expressed very little NANOG (Fig. 5C), although some expressed endoderm markers (CK19), mesoderm markers (desmin, αSMA), and ectoderm markers (βIII-tubulin, GFAP) at various levels (Fig. 5C). These results indicated that the DMC-hiPSCs were fully pluripotent in vitro.

In Vivo Differentiation of DMC-hiPSCs

The pluripotency of the DMC-hiPSCs was also evaluated by an in vivo teratoma formation assay. DMC-hiPSCs formed tumor masses in NOG mice after several months, and these tumor masses contained histological components of the three germ layers. Some tumors showed neuroepithelial-like structures that expressed human NCAM (ectoderm) (Fig. 6). The tumors also showed blood vessels and fibrous stroma that were positive for human vimentin, muscle-like structures that expressed desmin (mesoderm), and gut-like epithelium that was positive for epithelial membrane antigen (EMA) or cytokeratin (endoderm) (Fig. 6). Thus, the DMC-hiPSCs formed teratomas showing in vivo pluripotency, which indicated that the DMC-hiPSCs met the criteria for hiPSCs.

Gene Expression Profile of DMC-hiPSCs

To further characterize the DMC-hiPSCs at the molecular level, we examined the genome-wide gene expression profile of two DMC-hiPSCs in comparison to those of hESCs and the parental DMCs. Microarray analysis verified that there was a large difference in the transcriptome profile between the DMC-hiPSCs and parental DMCs and, in contrast, a strong similarity between that of the DMC-hiPSCs and KhES1 (Fig. 7A). Many undifferentiated ES cell marker genes (2), such as OCT3/4 (POU5F1), SOX2, NANOG, TERT, FOXD3, growth differentiation factor 3 (GDF3), zinc finger protein 42 homolog (ZFP42/reduced expression protein 1 [REX-1]), and teratocarcinoma-derived growth factor 1 (TDGF1), were expressed in the DMC-iPSCs at the same level as in the hESCs (Table 3), although these transcripts were not detected in the parental DMCs.

Among the 108 probe sets in the Human Genome U133 plus 2.0 Array for characterizing undifferentiated stem cells (2), the expression of the X (inactive)-specific transcript (nonprotein coding) gene (XIST) in one of the DMC-iPSCs (DMC5403) was more than 10 times that in the hESCs and was the same as in the parental DMCs (Table 3). Quantitative RT-PCR analysis for the XIST gene expression showed that the expansion and continuous passage of DMC-iPSCs led to the loss of XIST transcription in clone DMC5403 (Fig. 7B). The other DMC-iPSC clone (DMC5413) and a female DFB-iPS clone expressed XIST at a very low level at the beginning of culture (less than 10 passages) and after many passages (no less than 27 passages) (Fig. 7B). The methylation status of the XIST promoter region was assessed by methylation-specific PCR. Genomic DNA extracted from the parental female cells and DMC-hiPSC clone 5403 produced similar amounts of PCR products with both methylated and unmethylated DNA-specific primer sets. In contrast, the methylated DNA-specific primer set produced almost all the amplified products from the other clone, 5413, and the female DFB-hiPSCs (Fig. 7C).

Recently, new key molecules for efficient reprogramming, lung carcinoma-derived Myc (MYCL1) and glioma-associated oncogene similar protein [GLIS] family zinc finger (GLIS1), were reported (24,36). We evaluated the expression of these genes and of other GLI-related Krüppel-like zinc finger genes, GLIS2 and GLIS3, in several cell lines and tissues (Fig. 8A). Quantitative RT-PCR analysis showed that MYCL1 was expressed in all the primary cells, with the DFBs expressing three to four times the level observed in the placenta-derived cells or BM-MSCs. GLIS1 expression was detected in the testis at a high level and in the placenta at a moderate level. Of the primary cells, a low level of GLIS1 expression was detected in only the AECs and DMCs; no significant expression of GLIS1 was detected in the hESCs or hiPSCs. On the other hand, significant amounts of GLIS2 and GLIS3 were expressed in the placenta-derived cells, DFBs, and BM-MSCs, while very low levels were expressed in pluripotent stem cells, testis, and placenta (Fig. 8A). Seventeen factors that can substitute for Klf4 have been identified, although they have much lower efficiencies in iPSC generation (24). Among these factors, we evaluated Zinc finger and SCAN domain containing 4 (Zscan4), which is expressed exclusively in mouse late

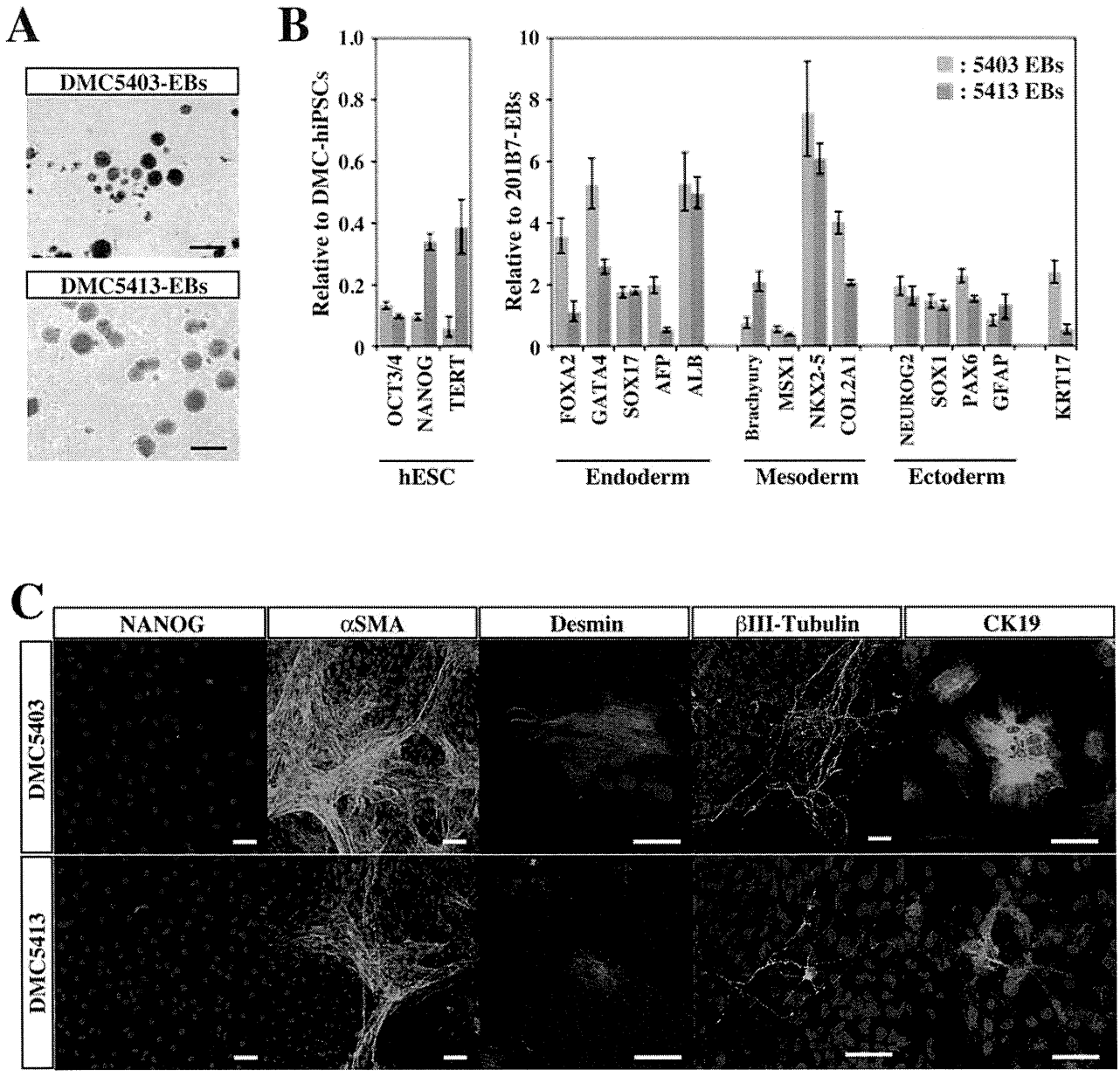

Figure 5. In vitro differentiation of DMC-hiPSCs. (A) Embryoid bodies (EBs) derived from two DMC-hiPSC clones on day 10. Scale bar: 200 μm. (B, left) Expression of human pluripotent stem cell marker genes in the same EBs on day 10 in suspension culture compared with their corresponding DMC-hiPSCs. (Right) Differentiation-specific marker gene expression relative to that of EBs derived from 201B7. (C) Immunofluorescence staining of differentiated cells in Dulbecco's modified Eagle's medium (DMEM) containing 10% fetal bovine serum (FBS) for an additional 2 weeks. Scale bars: 50 μm. See Table 1 for gene definitions.

two-cell embryos and embryonic stem cells (7). ZSCAN4 expression was detected in five primary cultured cells at very low levels, but was roughly five times higher in AECs and DFBs than in AMCs, DMCs, or BM-MSCs (Fig. 8A). We also examined the expression of GLIS1 and ZSCAN4 in DFBs and DMCs 3 days after the transduction of OSKM. Under this condition, we observed an increase in ZSCAN4 but not in GLIS1 expression in both DFBs and DMCs (Fig. 8B).

DISCUSSION

DMCs Are a Promising Human Allogeneic Cell Type for Generating hiPSCs

In this study, we demonstrated that hiPSCs were efficiently generated from DMCs, which were derived from the maternal components of placental tissue. The DMC-hiPSCs maintained a normal karyotype and showed equivalent characteristics to hESCs in colony morphology, global gene expression profile (including human

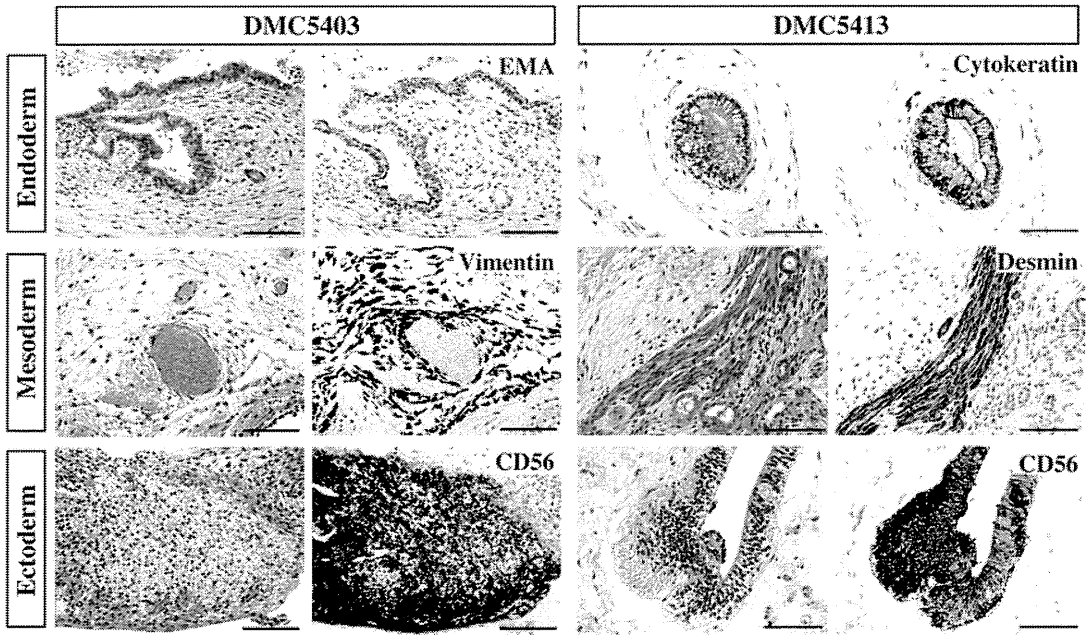

Figure 6. In vivo differentiation of DMC-hiPSCs. Teratomas derived from two DMC-hiPSCs (DMC5403, DMC5413) were examined by H&E and immunohistochemical staining. Teratomas from both DMC-hiPSCs contained histological components of the three germ layers, including neuroepithelial structures expressing human neural cell adhesion molecule (NCAM) (CD56, ectoderm), blood vessels and fibrous stroma-like structures expressing human vimentin or muscle-like structures expressing desmin (mesoderm), and gut-like epithelium expressing epithelial membrane antigen (EMA) or AE1 and AE3 (endoderm). Scale bars: 100 μm.

pluripotent stem cell markers), and DNA methylation status of the OCT3/4 and NANOG promoters, although these iPSC clones showed minor differences from each other in gene expression patterns and in the methylation status of promoter regions. In addition, the DMC-hiPSCs were able to differentiate into components of the three germ layers in vitro and in vivo. These data indicated that the DMC-hiPSC clones acquired full pluripotency equal to that of hiPSCs derived from DFBs or other cell sources and that the generation of iPSCs from DMCs is feasible.

The overall efficiency of reprogramming DMCs was almost the same as for DFBs, the most commonly used primary cell type for generating hiPSCs. However, we found several differences between DMCs and DFBs in the present study. In comparison with DFBs, DMCs formed about half the number of ALP^+ colonies (Fig. 2B, top). However, about 90% of the hESC-like colonies from DMCs were fully reprogrammed, while fewer than 40% of those from DFBs were successfully reprogrammed (Fig. 2B, bottom). Consequently, the overall reprogramming efficiency of DMCs was comparable to that of DFBs. There are various possible reasons for this higher reprogramming efficiency of DMCs. First, given that DMCs expressed the amphotropic retrovirus-introduced transgenes at two to three times the level expressed by DFBs (Fig. 2A), DMCs may be particularly compatible with this gene transduction system. Second, the endogenous gene expression profile of DMCs might result in improved reprogramming efficiency. Many previous reports have indicated that OSKM are important for reprogramming cells to iPSCs and that the endogenous expression of any of the four factors can reduce the number of genes needed for reprogramming (6,19,35). Furthermore, recently reported key molecules for efficient reprogramming, MYCL1 and GLIS1 (24,36), were expressed by the DMCs.

Our quantitative RT-PCR analysis showed that, among the four reprogramming factors (OSKM), only c-MYC was expressed in DMCs at the same level as in hESCs, similar to other placenta-derived cells and DFBs (Fig. 1). However, expression of the GLIS1 gene was detected only in the testis, placenta, and their derivative cells, the AECs and DMCs (Fig. 8). The transduction of GLIS1 along with OCT3/4, KLF4, and SOX2 markedly increases the expression of several genes that enhance iPSC generation, including lin-28 homolog A (*C. elegans*; LIN28A) (47), NANOG (38), neuroblastoma-derived Myc (MYCN), and MYCL1 (31), and the number of fully reprogrammed cells (24). The low endogenous expression of GLIS1 in the DMCs, combined with the efficient retroviral gene transduction, might contribute to the higher efficiency of DMC reprogramming.

On the other hand, the level of MYCL1 expression in the three placenta-derived cell types was low compared to that in DFBs (Fig. 8A). It is well known that DFBs can be reprogrammed efficiently by three (OSK)

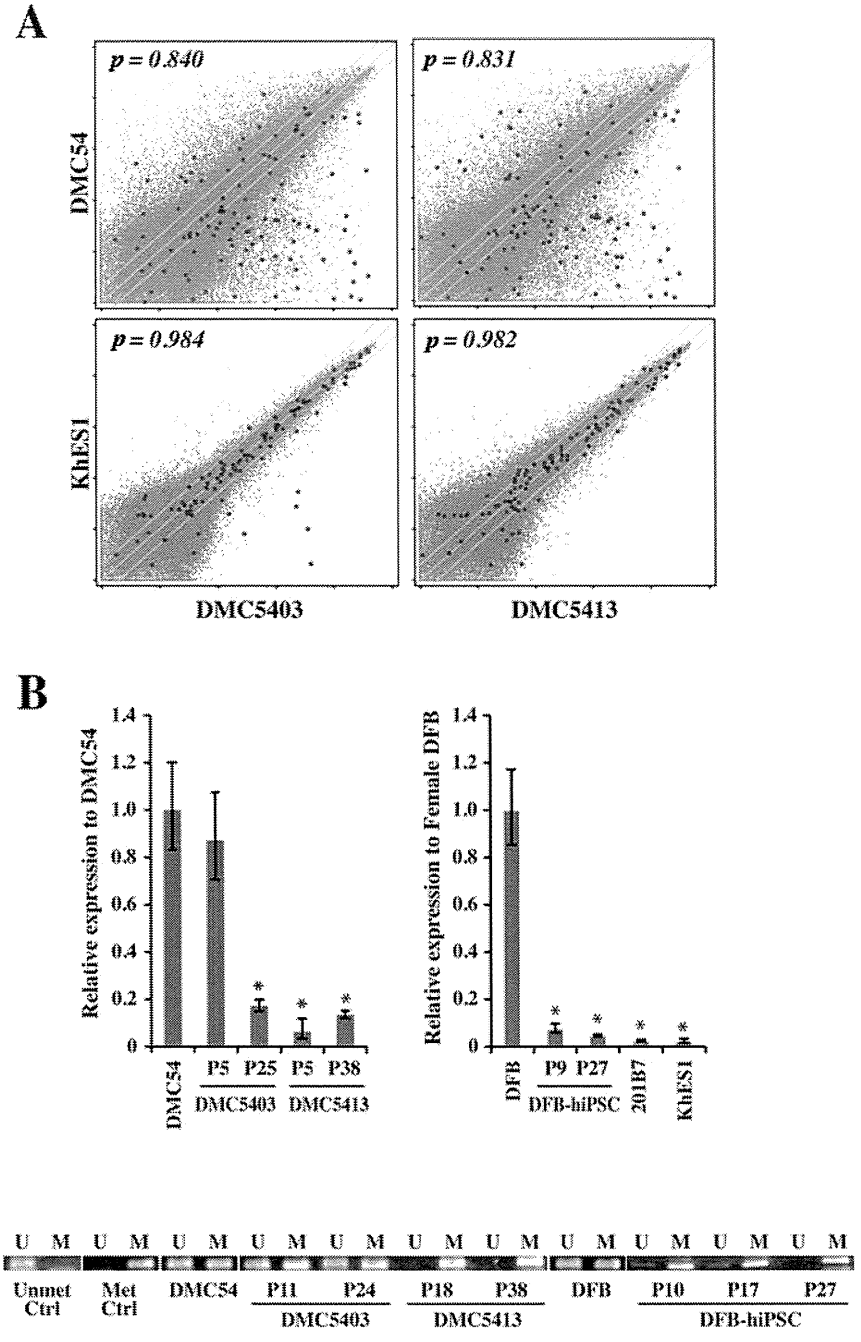

Figure 7. Transcriptional expression analysis of DMC-hiPSCs. (A) Scatter plots comparing the DNA microarray analysis data between DMC-iPSCs and parental DMCs (top) and between DMC-hiPSCs and human ES cells (KhES1) (bottom). The diagonal lines indicate twofold changes between the two samples, and the Pearson's coefficients are shown in the scatter plots. Red dots indicate data from probe sets for characterizing undifferentiated stem cells (see Table 1). (B) qRT-PCR analysis of X (inactive)-specific transcript (XIST) gene expression in female cells. Data are presented as the value relative to parental DMCs or DFBs. (C) Methylation-specific PCR was performed to examine the methylation status of the XIST promoter. The PCR products were specific for the methylated (M) or unmethylated (U) genome.

Table 3. Gene Expression Data of the Probe Sets in the Affymetrix Human Genome U133 Plus 2.0 Array for the Characterization of Undifferentiated Stem Cells

				Flag[a]				Fold Change Versus DMC54		Fold Change Versus KhES1	
Probe Set ID	UniGene ID	Gene Title	Symbol	DMC54	DMC5403	DMC5413	KhES1	DMC5403	DMC5413	DMC5403	DMC5413
1552982_a_at	Hs.1755	Fibroblast growth factor 4	FGF4	A	A	A	A	1.8	2.6	1.5	2.2
1554776_at	Hs.335787	Zinc finger protein 42 homolog (mouse)	ZFP42	A	P	P	P	84.4	75.3	−1.2	−1.4
1554777_at	Hs.335787	Zinc finger protein 42 homolog (mouse)	ZFP42	A	P	P	P	126.1	220.4	−1.5	1.2
1555271_a_at	Hs.492203	Telomerase reverse transcriptase	TERT	A	A	A	M	4.1	3.0	1.1	−1.2
1560469_at	Hs.33446	Nuclear receptor subfamily 5, group A, member 2	NR5A2	A	P	A	A	33.0	2.7	11.4	−1.1
1569689_s_at	Hs.302352	γ-Aminobutyric acid (GABA) A receptor, β3	GABRB3	A	A	A	A	1.6	−1.3	1.6	−1.3
201005_at	Hs.114286	CD9 molecule	CD9	P	P	P	P	2.2	2.8	1.1	1.4
201315_x_at	Hs.709321	Interferon-induced transmembrane protein 2 (1-8D)	IFITM2	P	P	P	P	−1.6	−1.2	1.5	1.9
201578_at	Hs.723993	Podocalyxin-like	PODXL	P	P	P	P	8.7	7.8	1.2	1.1
201601_x_at	Hs.458414	Interferon-induced transmembrane protein 1 (9-27)	IFITM1	P	P	P	P	3.9	4.5	1.7	1.9
202575_at	Hs.405662	Cellular retinoic acid binding protein 2	CRABP2	A	P	P	P	7.5	25.7	−2.7	1.3
204053_x_at	Hs.500466	Phosphatase and tensin homolog	PTEN	P	P	P	P	−1.3	−1.3	1.0	1.0
204054_at	Hs.500466	Phosphatase and tensin homolog	PTEN	P	P	P	P	−2.2	−2.1	−1.0	1.0
204271_s_at	Hs.82002	Endothelin receptor type B	EDNRB	A	P	P	P	596.2	435.3	2.2	1.6
204273_at	Hs.82002	Endothelin receptor type B	EDNRB	A	P	P	P	514.5	609.4	2.8	3.3
204535_s_at	Hs.631513	RE1-silencing transcription factor	REST	A	A	A	A	−3.2	−1.1	−1.1	2.7
204863_s_at	Hs.532082	Interleukin 6 signal transducer (gp130, oncostatin M receptor)	IL6ST	P	A	A	A	−11.8	−7.5	−1.4	1.1
204864_s_at	Hs.532082	Interleukin 6 signal transducer (gp130, oncostatin M receptor)	IL6ST	P	A	A	P	−10.1	−1.2	−7.3	1.1
205051_s_at	Hs.479754	v-Kit Hardy-Zuckerman 4 feline sarcoma viral oncogene homolog	KIT	P	P	P	P	9.1	10.8	−1.6	−1.4
205603_s_at	Hs.226483	Diaphanous homolog 2 (Drosophila)	DIAPH2	P	P	P	P	29.9	17.6	1.3	−1.3
205726_at	Hs.226483	Diaphanous homolog 2 (Drosophila)	DIAPH2	P	P	P	P	4.2	4.1	1.0	−1.0
205850_s_at	Hs.302352	γ-Aminobutyric acid (GABA) A receptor, β3	GABRB3	A	P	P	P	44.4	50.6	−1.4	−1.2
205876_at	Hs.133421	Leukemia inhibitory factor receptor α	LIFR	A	P	A	P	3.4	1.5	−1.0	−2.3
206012_at	Hs.520187	Left-right determination factor 2	LEFTY2	A	P	P	P	970.9	465.7	1.1	−1.9
206268_at	Hs.724790	Left-right determination factor 1	LEFTY1	A	P	P	P	342.1	155.5	1.2	−1.8
206286_s_at	Hs.385870	Teratocarcinoma-derived growth factor 1 teratocarcinoma-derived growth factor 3, pseudogene	TDGF1 TDGF3	A	P	P	P	12405.4	9524.5	1.4	1.1
206701_x_at	Hs.82002	Endothelin receptor type B	EDNRB	A	P	P	P	197.9	108.6	2.7	1.5
206783_at	Hs.1755	Fibroblast growth factor 4	FGF4	A	P	P	P	24.5	31.9	1.1	1.5
206805_at	Hs.252451	Sema domain, immunoglobulin domain (Ig), short basic domain, secreted, (semaphorin) 3A	SEMA3A	P	P	P	P	2.4	1.2	1.3	−1.4
207199_at	Hs.492203	Telomerase reverse transcriptase	TERT	A	P	P	P	3.0	3.9	−1.8	−1.4

(*continued*)